analytical chemistry

pubs.acs.org/ac Letter

Model, Simulation, and Experiments on Moving Exchange Boundary via Ligand and Quantum Dots in Chip Electrophoresis

Qiang Zhang,[+] Zehua Guo,[+] Fang Luo, Hua Xiao, Weiwen Liu,* Liuyin Fan,* and Chengxi Cao*

Cite This: *Anal. Chem.* 2021, 93, 5360−5364 Read Online

ACCESS | Metrics & More | Article Recommendations | Supporting Information

ABSTRACT: Herein, the quench model of the moving exchange boundary (MEB) was first created via a ligand of 5,5′-dithiobis(2-nitro-benzoic acid) (DTNB) and group of 3-mercaptopropionic acid (MPA) capped on QDs, and then the recovery model was formed via MPA and 2-nitro-5-thiobenzoic acid (TNB) capped on QDs. The theory on MEB dynamics and width was developed based on the two reversible models, the simulation was conducted for the illumination of MEB, and the protocol was described for the MEB runs. The experiments revealed that (i) the quench model could be created via DTNB and MPA capped on QDs and the recovery one could be *in situ* formed via MPA and TNB capped on QDs, showing the feasibility of MEB models; (ii) the simulations on MEB dynamics and width were in coincidence with the theoretic predictions, showing the validity of two models; and (iii) the experiments demonstrated the validity of models, predictions, and simulations. The models and theory have potential for development of a biosensor, nanoparticle characterization, separation science, and an affinity assay of ligand-QDs.

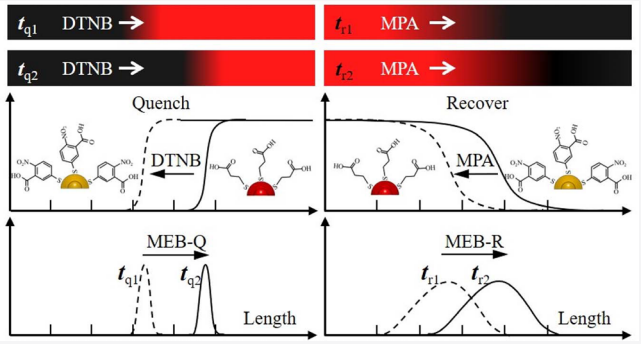

Electrophoretic techniques have played a key importance in the fields of life science, biomedicine, and bio/nanoparticles.[1−8] They have been used for genomic sequence,[1] protein separation and identification,[2] and drug/enzyme screenings.[3] Particularly, they have been applied for separation, capture, identification, and characteristics of bio/nanoparticles, e.g., mitochondrion,[4] microorganism,[5] exosomes,[6] and nanoparticles (NPs)[7] as well as quantum dots (QDs).[8]

The research of the electrolyte boundary has played a fundamental role for the development of electrophoresis. For example, the study on the moving boundary system (MBS) led to the creation of isotachophoresis (ITP), displacement electrophoresis,[9,10] and online sample stacking.[11] The application of concentration boundary to capillary electrophoresis resulted in the design of field amplified sample injection stacking.[12,13] The acid−base boundary created via electrolysis of salt was the classic model of isoelectric focusing (IEF).[13,14]

The moving reaction front[15−17] has opened the fantastic window of the moving reaction boundary (MRB).[8,13] First, the concept of MRB reactivated the development of IEF dynamics and the method.[13,18] Second, it initiated the electrophoretic biosensing for food safety.[19] Third, it induced the MRB-based sensing of hemoglobin A1c in diabetes blood[20] and accounting ligands on QDs.[8] However, there was a rare report on the model and simulation on moving exchange boundary (MEB).

Herein, the quench model of MEB-Q was first created via 5,5′-dithiobis(2-nitro-benzoic acid) (DTNB) and 3-mercaptopropionic acid (MPA) capped QDs, and the recovery model of MEB-R was *in situ* formed via MPA and 2-nitro-5-thiobenzoic acid (TNB) capped QDs due to their common surface ligands on QDs.[21−23] The theory on boundary dynamics and width was developed based on the models, and the simulation was conducted for explaining MEB dynamics and width, and the protocol was shown for the relevant experiments. The below experiments validated the models, theory, and simulation. The models and theory herein have potential to biosensor invention, NPs characteristics, separation creation, and affinity analysis of ligand-QDs.

RESULTS AND DISCUSSION

Quench Model of MEB-Q. Figure 1A and Figure S3 show the quench model of MEB-Q formed via DTNB and MPA capped on QDs (*viz.*, [MPA-QDs]). Unlike free MPA, the symbol of "-" in MPA-/[MPA-QDs] implies the MPA capped on QDs via the Zn−S_{thiol} bond or the S−S_{thiol} bond, etc.).[21] In the model, [MPA-QDs] with red fluorescence is fixed via gel, and DTNB (an anion) is set in the left well of capillary. Under

Received: January 18, 2021
Accepted: March 4, 2021
Published: March 23, 2021

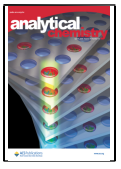

https://doi.org/10.1021/acs.analchem.1c00242
Anal. Chem. 2021, 93, 5360−5364

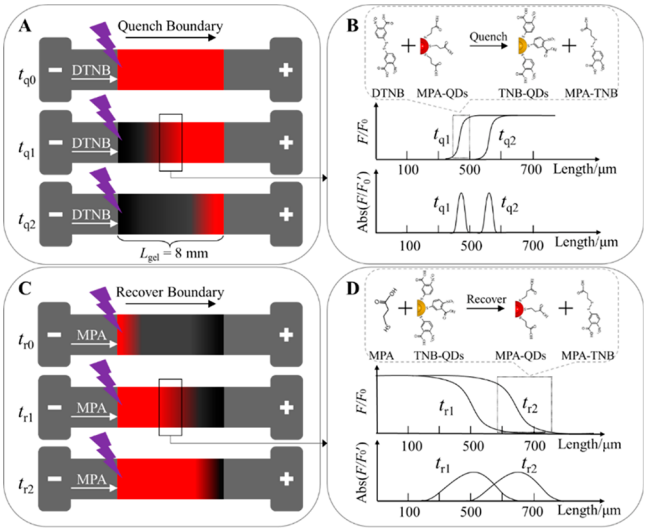

Figure 1. Models of MEB. Quench model of MEB-Q created via DTNB and MPA- capped on QDs in gel (A); exchange in MEB-Q and boundary curves of fluorescence and their derivatives (B); recovery model of MEB-R via MPA and TNB-exchanged onto QDs (C); exchange in recovery boundary and boundary curves of fluorescence and their derivatives (D). The F/F_0 is the normalized fluorescence intensity of boundary and F/F_0' is the derivative of the fluorescence intensity with respect to length.

an electric field, DTNB moves toward the anode, exchanges the MPA- on QDs, and leads to yield of [TNB-QDs]. DTNB can quench the fluorescence of [MPA-QDs] thanks to its benzene ring with a strong electron withdrawing effect.[22] As a result, DTNB displaces the group of MPA- on QDs via the following exchange,[23]

$$\text{[MPA-QDs]} + \text{DTNB} \overset{k_{1,-1}}{\longleftrightarrow} \text{[TNB-QDs]} + \text{MPA-TNB} \tag{I}$$

where [MPA-QDs] and [TNB-QDs] have, respectively, red and no fluorescence if 360 nm UV excites.[22] Consequently, Exchange (I) creates a fluorescent MEB-Q due to the fluorescence quench of [MPA-QDs].

In the quench mode, there is always an equivalent balance between DTNB and MPA- on QDs. As a run continues, more DTNB is forced into the zone of [MPA-QDs], and more MPA- is exchanged from [MPA-QDs] by DTNB, quenching [MPA-QDs] fluorescence. The motion of MEB-Q[8,19] is described via,

$$d_{\text{MEB-Q}} = v_{\text{MEB-Q}}(t_{q2} - t_{q1}) \tag{1}$$

where $d_{\text{MEB-Q}}$ is the migration distance of MEB-Q from the initial time of t_{q1} and the end time of t_{q2}, $v_{\text{MEB-Q}}$ is the moving rate of MEB-Q,

$$v_{\text{MEB-Q}} = -\frac{v_{\text{DTNB}} c_{\text{DTNB}}}{c_{\text{MPA-}} - c_{\text{DTNB}}} \tag{2}$$

where the $c_{\text{MPA-}}$ and c_{DTNB} are contents of MPA- on QDs and DTNB in the channel, respectively. However, the exchange of (I) is slow, the balance of interaction takes long time, and the MEB-Q is wide and blurry, indicating difficulty of exact readout of boundary location if without proper boundary definition (sections S2 and S3). This is evidently different from the sharp neutralization boundary.[8,19] In MEB-Q, the distributions of bound MPA- on QDs, free DTNB, bound TNB- on QDs, and free MPA among the motion direction of MEB-Q can be described via eqs S9−S12 in line with the previous work.[24] The analytical solutions of eqs S9−S12 are given in the details of eqs S21−S28. The product of MPA-TNB within MEB is removed from the surface of [TNB-QDs] at low content ($c_{\text{DTNB}} \gg c_{\text{MPA-TNB}}$). eqs S21−S28 indicate that if the content of MPA- on QDs is constant, the higher content of DTNB creates a higher exchange rate and a faster MEB-Q, and *vice versa*.

As early as in 1930s, McInnes et al.[9] defined the widths of MBS. In 2008, Khurana et al.[24] redefined the width via eq S29, showing the relation of the boundary width and rate. However, eq S29 cannot be used for describing MEB width due to the slow exchange of (I).[21] Thus, the width of MEB-Q is defined as the semiempirical equation (section S2),

$$w_{\text{MEB-Q}} = f(c_{\text{DTNB}}, c_{\text{MPA-}}, k)\frac{1}{v_{\text{MEB-Q}}} \tag{3}$$

where $f(c_{\text{DTNB}}, c_{\text{MPA-}}, k)$ is a comprehensive factor, representing the effect of diffusion, QDs size, gel retardation, and ligand exchange rate, etc. The width of $w_{\text{MEB-Q}}$ can be obtained from the MEB-Q run according to the curve derivative (Figure S2A), and $v_{\text{MEB-Q}}$ can be calculated by two adjacent peaks of t_{q1} and t_{q2} in Figure 1B. Hence the factor can be obtained via experimental data and considered as a constant for convenience (Section S2−S4).

eq 3 shows the reverse relation of boundary rate and width, including the concentrations of DTNB and MPA-. When the electrical intensity and other conditions (QDs size and gel pore etc.) are constant, the $v_{\text{MEB-Q}}$ is related with the concentrations of DTNB and MPA-. If the concentration of [MPA-QDs] is constant, the higher content of DTNB is corresponding to a faster rate of MEB-Q and a sharper boundary and *vice versa*.

Recovery Model of MEB-R. To demonstrate the exchangeability of MEB, it is necessary to show the quenched QDs in Figure 1A,B can be *in situ* recovered via MPA. In Figure 1C, the sample zone is filled with MPA after the quench exchange. When the electric field is reapplied, MPA is driven into the zone of [TNB-QDs] and exchanges TNB- from [TNB-QDs], leading to the reverse exchange,[23]

$$\text{[TNB-QDs]} + \text{MPA} \overset{k_{2,-2}}{\longleftrightarrow} \text{[MPA-QDs]} + \text{MPA-TNB} \tag{II}$$

Hence, after the TNB- on QDs is displaced via MPA, the fluorescence of QDs is recovered.[22] Clearly, MEB-R is the reverse of MEB-Q. The rate of MEB-R can be written as

$$v_{\text{MEB-R}} = -\frac{v_{\text{MPA}} c_{\text{MPA}}}{c_{\text{TNB-}} - c_{\text{MPA}}} \tag{4}$$

The concentration of bound MPA-, TNB-MPA, bound TNB-, and free MPA among the moving direction of MEB-R can be, respectively, described via eqs S35−S38. The analytical solutions of eqs S35−S38 are given as eqs S39−S44, implying that if the content of TNB- on QDs is constant, the higher content of MPA creates a higher exchange rate and a faster exchange boundary and *vice versa*.

The semiempirical width of MEB-R is defined as

$$w_{\text{MEB-R}} = f(c_{\text{MPA}}, c_{\text{TNB-}}, k)\frac{1}{v_{\text{MEB-R}}} \tag{5}$$

where $f(c_{\text{MPA}}, c_{\text{TNB-}}, k)$ is a comprehensive factor, being similar to the one of $f(c_{\text{DTNB}}, c_{\text{MPA-}}, k)$ in eq 3. Equation 5 indicates

https://doi.org/10.1021/acs.analchem.1c00242
Anal. Chem. 2021, 93, 5360−5364

that the higher the MPA content is, the faster the moving rate appears and the sharper the MEB-R is and *vice versa*.

Simulations on MEB-Q. Figure 2A1−A3 and Figure S10 reveal the simulations on MEB-Q created with 100 μM DTNB and 2.5 μM [MPA-QDs] under the times of 30−150 s. Panel A1 showed that the content of DTNB among the channel under the given times, but the others of MPA- (*viz.*, the relative fluorescence intensity (RFI) of [MPA-QDs]), TNB- on QDs and MPA-TNB were so low that they could not be observed on the scale of 0.1 mM. Hence, panel A2 was given for showing the distributions of MPA-, TNB-, and MPA-TNB on the scale of 5.0 μM. Panel A3 showed the curve derivatives of MPA- distribution (equivalently, RFI of [MPA-QDs]) in panel A2, marking the location and width of RFI peaks in the times of 30−150 s. As shown in Figure 2A1−A3, MEB-Q moved evenly, validating the quench model and eq 2.

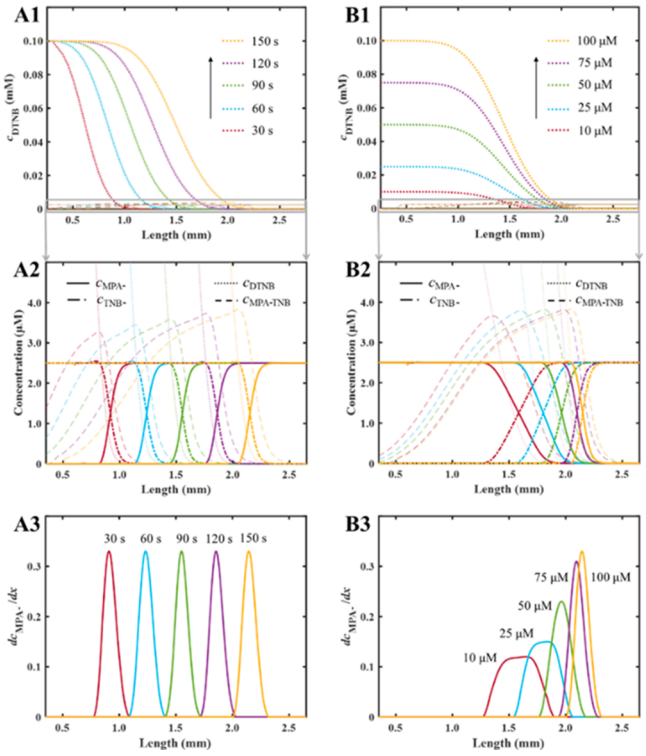

Figure 2. Simulations on distributions of MPA-, DNTB, TNB-, and MPA-TNB and boundary location and width within MEB-Q created via DTNB and MPA- on QDs. Distributions of DNTB during 30−150 s run of MEB-Q in 0.1 mM scale (A1); distributions of MPA- (*viz.*, RFI of [MPA-QDs]), TNB-, and MPA-TNB during 30−150 s run of MEB-Q in 5.0 μM scale (A2); and boundary curve derivative of MPA- distribution (*viz.*, RFI of [MPA-QDs]) in panel A2 (A3). Distributions of DNTB in 150 s MEB-Q under 10−100 μM DTNB at the 0.1 mM scale (B1); distributions of MPA-, TNB-, and MPA-TNB under 10−100 μM DTNB at the 5.0 μM scale (B2); and boundary curve derivative of MPA- distribution (*viz.*, RFI) in panel B2 (B3). The simulative conditions given in section S3 were the same as the experimental in sections S1 and S4.

Figure 2B1−B3 and S10 reveal the simulations on the quench boundary of 150 s run under the initial DTNB contents of 10−100 μM. Figure 2B1 exhibits the distribution of DTNB on the scale of 0.1 mM, and Figure 2B2 highlights the distributions of MPA- (*viz.*, RFI of [MPA-QDs]), TNB- on QDs, and MPA-TNB in panel 2B1. Figure 3B3 unveils the derivatives of MPA- distribution (*viz.*, RFI) and the position and thickness of MEB-Q under 10−100 μM DTNB. As evidently displayed in Figure 2B1−B3, a higher content DTNB induced a faster rate of MEB-Q, a thinner MEB, and *vice versa*. These simulations were obviously in agreement with the predictions of eqs 2 and 3 in Figures S4 and S5, further indicating the validity of MEB-Q, eq 2, and the semiempirical equation of eq 3.

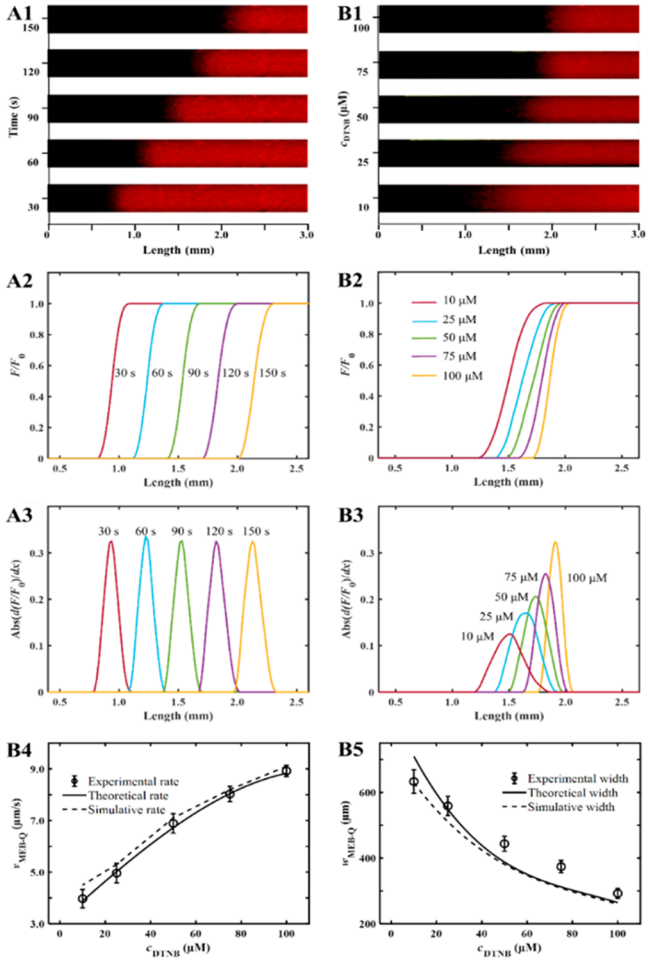

Figure 3. Experiments, analysis, and simulations on MEB-Q created via DTNB and [MPA-QDs]. Boundary motion image of 30−150 s MEB-Q of 100 μM DTNB and 2.5 μM [MPA-QDs] (A1); RFI of [MPA-QDs] (*viz.*, distribution of MPA-) in channel scanned from panel A1 (A2); derivatives of RFI in panel A2 (A3). Boundary motion image in 150 s MEB-Q formed via DTNB and [MPA-QDs] (B1); RFI of [MPA-QDs] in panel B1 (B2); derivative of RFI in panel B2 (B3). Comparisons of v_{MEB-Q} vs c_{DTNB} among experiments in panel B3, analysis of eqs 1 and 2 and simulation in Figure 2B3 (B4); comparisons of w_{MEB-Q} vs c_{DTNB} among experiments in panel B3, analysis of eq 3, and simulations in Figure 2B3 (B5). The optimized conditions are given in section S4.

Simulations on Model of MEB-R in Figure S11. Evidently, the even motion of MEB-R in Figure S11A1−A3 shows the validity of the recovery model and eq 4. Further, the boundary movement and width in Figure S11B1−B3 are clearly in coincidence with the predictions in Figures S7 and S8, denoting the validity of the MEB-R model, eq 4, and eq 5.

Experimental Demonstration on MEB-Q. Figure 3A1−A3 shows the experiments on the quench boundary created with 100 μM DTNB and 2.5 μM [MPA-QDs] in the times of 30−150 s. Figure 3A1 reveals the fluorescent imaging

https://doi.org/10.1021/acs.analchem.1c00242
Anal. Chem. 2021, 93, 5360−5364

(equivalently, the distribution of MPA- on QDs) of MEB-Q formed with DTNB and [MPA-QDs] within 30−150 s. Figure 3A2 presents the fluorescent quench of [MPA-QDs] (*viz.*, RFI or content distribution of MPA-) in channel scanned from the imaging in Figure 3A1. Figure 3A3 highlights the curve derivatives of fluorescence in Figure 3A2 and the location and width of MEB-Q. Figure 3A1−A3 presents the even moving rate of MEB-Q quantitatively validating the model, eq 2, and simulations in Figure 2A1−A3.

Figure 3B1−B3 further reveals the experiments on the 150 s MEB-Q formed with 2.5 μM [MPA-QDs] and 10−100 μM DTNB. Figure 3B1 shows the imaging of the boundary motion of MEB-Q. Figure 3B2 displays the fluorescent quenching of [MPA-QDs] scanned from the images in Figure 3B1. Figure 3B3 shows the derivatives of RFI (*viz.*, the concentration distribution of MPA-) in Figure 3B2. Figure 3B4 depicts the relationship of $v_{\text{MEB-Q}}$ vs c_{DTNB} from the data of Figure 3B3 and the fair agreement among the experiments in Figure 3B3, the analysis via eq 2, and the simulations in Figure 2B, further validating the model, eq 2, and the simulations. Particularly, Figure 3B5 unveils the relation of $w_{\text{MEB-Q}}$ vs c_{DTNB} from the data of Figure 3B3 and the fair coincidences among the experiments in Figure 3B3, analyses of eq 3, and simulations in Figure 2B3, quantitatively manifesting the quench model, eq 3, and simulations.

Experiments on MEB-R in Figure S13. Similarly, the comparisons in Figure S13B4 highly demonstrate the recovery model, eq 4, and the simulations in Figure S11. Finally, the comparisons of $w_{\text{MEB-R}}$ vs c_{MPA} in Figure S13B5 quantitatively manifest the model of MEB-R, eq 5, and simulations.

Figure 3B4,B5 and S13B4−S13B5 also show the discrepancy between the theoretical and experimental values. For example, the theoretical widths were generally less than the experimental. The possible reasons could be the symmetric models of MEB, the rough estimate of the reaction rate, electric field, solution conductivity, and others. Thus, more accurate models will be developed in the future.

MEB Potentials. The MEB models have the imaginary potentials to biosensor design, nanomaterials characteristics, and separation creation, etc. First, the models had potential for biosensing. The concept of MRB has initiated the biosensing of protein in milk,[19] glycoprotein in blood,[20] and miRNA in cancer samples.[25] The experiments herein implied the potential sensing of star molecules of glutathione.

Second, the models had potential to characterize NPs. Identification of the ligand (e.g., MPA- on NPs) via NMR still faced challenges: (i) impossibility of NPs analyses via NMR if without an ultrapure inner standard, (ii) expensive instrument, and (iii) complex sample pretreatment. The challenges were addressed by the MRB concept.[8] Figure 3 and ref 8. indicate an alternative potential to NPs characterization.

Third, the models indicated the potential for separative science. Initially, Deman[16] and Dee[17] observed the separation of metal ions via solubility products in MRB. The authors showed the efficient separation of proteins in line with p*I*s in MRB.[13] Zhang et al.[26] unveiled the separation of metal ions via chelation constants. The experiments herein might indicate a novel separation in line with exchange constants.

Fourth, the models had significance to the affinity assay of ligand-QDs. Nonequilibrium affinity capillary electrophoresis has been used for affinity constant analysis, aptamer evolution, and ligand selection.[27,28] The models here implied partial nonequivalent interaction of ligand-QDs and have the potential for affinity assays.

CONCLUSIONS

The following conclusions were achieved. First, the quench model of MEB was developed by using DTNB and [MPA-QDs], and then the recovery model was *in situ* created via MPA and [TNB-QDs]. Second, the relevant theories of boundary dynamics and width were advanced based on the two models. Third, the simulations were conducted for the illumination on the dynamics and widths of the quenching and recovery MEBs. Fourth, the protocols were developed for the experiments of MEB. Fifth, the experiments validated the MEB models and simulations and predictions. The models, theory, simulations, and protocols have the potential for the development of an electrophoresis biosensor, determine the characteristics of NPs, and separation science coupled with affinity analysis of ligand-QDs, etc.

ASSOCIATED CONTENT

Supporting Information

The Supporting Information is available free of charge at https://pubs.acs.org/doi/10.1021/acs.analchem.1c00242.

Experimental section of chemicals, apparatus, and MEB procedures; theoretical section of quench model of MEB-Q and recovery model of MEB-R; numerical simulation of assumption, simulation model, and boundary conditions; optimization of experimental conditions; signal process; simulation results; and experiments on recovery boundary (PDF)

AUTHOR INFORMATION

Corresponding Authors

Chengxi Cao − *Department of Instrument Science and Engineering, School of Electronic Information & Electrical Engineering, School of Life Science and Biotechnology, State Key Laboratory of Microbial Metabolism, and Shanghai Sixth People's Hospital, Shanghai Jiao Tong University, Shanghai 200240, China;* orcid.org/0000-0002-3873-5112; Email: cxcao@sjtu.edu.cn

Weiwen Liu − *Department of Instrument Science and Engineering, School of Electronic Information & Electrical Engineering, Shanghai Jiao Tong University, Shanghai 200240, China*; Email: weiwenliu@sjtu.edu.cn

Liuyin Fan − *Student Innovation Center, Shanghai Jiao Tong University, Shanghai 200240, China*; Email: lyfan@sjtu.edu.cn

Authors

Qiang Zhang − *Department of Instrument Science and Engineering, School of Electronic Information & Electrical Engineering, Shanghai Jiao Tong University, Shanghai 200240, China*

Zehua Guo − *Department of Instrument Science and Engineering, School of Electronic Information & Electrical Engineering, Shanghai Jiao Tong University, Shanghai 200240, China*

Fang Luo − *School of Life Science and Biotechnology, State Key Laboratory of Microbial Metabolism, Shanghai Jiao Tong University, Shanghai 200240, China*

Hua Xiao − *School of Life Science and Biotechnology, State Key Laboratory of Microbial Metabolism, Shanghai Jiao*

https://doi.org/10.1021/acs.analchem.1c00242
Anal. Chem. 2021, 93, 5360−5364

Tong University, Shanghai 200240, China; orcid.org/0000-0002-2831-0436

Complete contact information is available at: https://pubs.acs.org/10.1021/acs.analchem.1c00242

Author Contributions

[+]Q. Zhang and Z.-H. Guo have equal contribution to the work. Q. Zhang developed the mathematic and digital models and performed the simulation, part of the protocol, part of the discussion, and part of the manuscript preparation. Z.-H. Guo conducted part of the protocol, all of the experiments and data analyses, most of the discussion, and most of the manuscript preparation.

Notes

The authors declare no competing financial interest.

■ ACKNOWLEDGMENTS

This work was supported by grants from the National Natural Science Foundation of China (Grant Nos. 31727801 and 22074091).

■ REFERENCES

(1) Schafer, A. J.; Hawkins, J. R. *Nat. Biotechnol.* **1998**, *16* (1), 33−39.
(2) Bikos, D. A.; Mason, T. G. *Nat. Commun.* **2019**, *10*, 3631.
(3) Pereira, S. A. P.; Dyson, P. J.; Saraiva, M. L. M. F. S. *TrAC, Trends Anal. Chem.* **2020**, *126*, 115862.
(4) Eubel, H.; Lee, C. P.; Kuo, J.; Meyer, E. H.; Taylor, N. L.; Millar, A. H. *Plant J.* **2007**, *52*, 583−594.
(5) Jiang, X. T.; Liu, S.; Zhang, Y.; Ji, Y.; Sohail, A.; Cao, C. X.; Wang, P.; Xiao, H. *Anal. Chem.* **2020**, *92* (17), 12017−12025.
(6) Ayala-Mar, S.; Perez-Gonzalez, V. H.; Mata-Gomez, M. A.; Gallo-Villanueva, R. C.; Gonzalez-Valdez, J. *Anal. Chem.* **2019**, *91* (23), 14975−14982.
(7) Chinappi, M.; Yamaji, M.; Kawano, R.; Cecconi, F. *ACS Nano* **2020**, *14* (11), 15816−15828.
(8) Zhang, Q.; Liu, W. W.; Khan, M. I.; Wang, C. H.; Li, G. Q.; Xiao, H.; Wang, Y. X.; Cao, C. X. *Anal. Chem.* **2019**, *91* (12), 7500−7504.
(9) MacInnes, D. A.; Longsworth, L. *Chem. Rev.* **1932**, *11* (2), 171−230.
(10) Beckers, J. L.; Verheggen, T. P.; Everaerts, F. M. *Isotachophoresis: Theory, Instrumentation and Applications*; Elsevier, 1976.
(11) Krauss, S. T.; Ross, D.; Forbes, T. P. *Anal. Chem.* **2019**, *91* (20), 13014−13021.
(12) Crosnier de Lassichère, C. d.; Mai, T. D.; Otto, M.; Taverna, M. *Anal. Chem.* **2018**, *90* (4), 2555−2563.
(13) Cao, C. X.; Fan, L. Y.; Zhang, W. *Analyst* **2008**, *133* (9), 1139−1157.
(14) Righetti, P. G.; Drysdale, J. W. *J. Chromatogr. A* **1974**, *98* (2), 271−321.
(15) Onsager, L. *Science* **1969**, *166* (3911), 1359−1364.
(16) Deman, J. *Anal. Chem.* **1970**, *42* (9), 983−989.
(17) Dee, G. *Phys. Rev. Lett.* **1986**, *57* (3), 275.
(18) Cao, C. X. *J. Chromatogr. A* **1998**, *813* (1), 153−171.
(19) Wang, C. H.; Zhang, Q.; Liu, X. P.; Li, G. Q.; Kong, H.; Khan, M. I.; Xiao, H.; Wang, Y. X.; Liu, W. W.; Cao, C. X. *Lab Chip* **2019**, *19* (3), 484−492.
(20) Wu, X. J.; Meng, Q. H.; Zhang, Q.; Fan, L. Y.; Xiao, H.; Cao, C. X. *Sens. Actuators, B* **2020**, *309*, 127773.
(21) Pong, B. K.; Trout, B. L.; Lee, J. Y. *Langmuir* **2008**, *24*, 5270−5276.
(22) do Nascimento, R. F.; Ferreira, O. P.; De Paula, A. J.; Neto, V. d. O. S. *Nanomaterials Applications for Environmental Matrices: Water, Soil and Air*; Elsevier, 2019.
(23) Koole, R.; Schapotschnikow, P.; de Mello Donegá, C.; Vlugt, T. J.; Meijerink, A. *ACS Nano* **2008**, *2* (8), 1703−1714.
(24) Khurana, T. K.; Santiago, J. G. *Anal. Chem.* **2008**, *80* (16), 6300−6307.
(25) Chen, L.; Zhang, Q.; Liu, W. W.; Xiao, H.; Liu, X. P.; Fan, L. Y.; Wang, Y. X.; Li, H. G.; Cao, C. X. *Biosens. Bioelectron.* **2021**, *171*, 112676.
(26) Zhang, W.; Guo, C. G.; Fan, L. Y.; Cao, C. X. *Analyst* **2013**, *138*, 5039−5051.
(27) Levay, A.; Brenneman, R.; Hoinka, J.; Sant, D.; Cardone, M.; Trinchieri, G.; Przytycka, T. M.; Berezhnoy, A. N. *Nucleic Acids Res.* **2015**, *43*, e82.
(28) Zhou, J. H.; Rossi, J. *Nat. Rev. Drug Discovery* **2017**, *16*, 181−202.